Design and implementation of a sub-nm resolution microspectrometer based on a Linear-Variable Optical Filter

Arvin Emadi,* Huaiwen Wu, Ger de Graaf and Reinoud Wolffenbuttel

Faculty EEMCS, Department ME/EI, Delft University of Technology, Mekelweg 4, 2628 CD, Delft, The Netherlands
**a.emadi@tudelft.nl*

Abstract: In this paper the concept of a microspectrometer based on a Linear Variable Optical Filter (LVOF) for operation in the visible spectrum is presented and used in two different designs: the first is for the narrow spectral band between 610 nm and 680 nm, whereas the other is for the wider spectral band between 570 nm and 740 nm. Design considerations, fabrication and measurement results of the LVOF are presented. An iterative signal processing algorithm based on an initial calibration has been implemented to enhance the spectral resolution. Experimental validation is based on the spectrum of a Neon lamp. The results of measurements have been used to analyze the operating limits of the concept and to explain the sources of error in the algorithm. It is shown that the main benefits of a LVOF-based microspectrometer are in case of implementation in a narrowband application. The realized LVOF microspectrometers show a spectral resolution of 2.2 nm in the wideband design and 0.7 nm in the narrowband design.

OCIS codes: (220.0220) Optical design and fabrication; (300.6190) Spectrometers; (310.4165) Thin films: Multilayer design.

References and links

1. R. F. Wolffenbuttel, "MEMS-based optical mini- and microspectrometers for the visible and infrared spectral range," J. Micromech. Microeng. **15**(7), S145–S152 (2005).
2. G. Minas, R. F. Wolffenbuttel, and J. H. Correia, "A lab-on-a-chip for spectrophotometric analysis of biological fluids," Lab Chip **5**(11), 1303–1309 (2005).
3. J. H. Correia, G. de Graaf, S. H. Kong, M. Bartek, and R. F. Wolffenbuttel, "Single-chip CMOS optical microspectrometer," Sens. Actuators A Phys. **82**(1-3), 191–197 (2000).
4. S. W. Wang, M. Li, C. S. Xia, H. Q. Wang, X. S. Chen, and W. Lu, "128 channels of integrated filter array rapidly fabricated by using the combinatorial deposition technique," Appl. Phys. B **88**(2), 281–284 (2007).
5. R. R. McLeod and T. Honda, "Improving the spectral resolution of wedged etalons and linear variable filters with incidence angle," Opt. Lett. **30**(19), 2647–2649 (2005).
6. A. Emadi, H. Wu, G. de Graaf, and R. F. Wolffenbuttel, "CMOS-compatible LVOF-based visible microspectrometer," Proc. SPIE **7680**, 76800W (2010).
7. A. Emadi, S. Grabarnik, H. Wu, G. de Graaf, K. Hedsten, P. Enoksson, J. H. Correia, and R. F. Wolffenbuttel, "Spectral measurement using IC-compatible linear variable optical filter," Proc. SPIE **7716**, 77162G (2010).
8. A. Emadi, H. Wu, S. Grabarnik, G. De Graaf, K. Hedsten, P. Enoksson, J. H. Correia, and R. F. Wolffenbuttel, "Fabrication and characterization of IC-compatible linear variable optical filters with application in a micro-spectrometer," Sens. Actuators A Phys. **162**(2), 400–405 (2010).
9. M. Born and E. Wolf, *Principles of Optics: Electromagnetic Theory of Propagation, Interference and Diffraction of Light*, 7th ed., 360–376 (Cambridge University Press, 1999).
10. A. Emadi, H. Wu, S. Grabarnik, G. de Graaf, and R. F. Wolffenbuttel, "Vertically tapered layers for optical applications fabricated using resist reflow," J. Micromech. Microeng. **19**(7), 074014 (2009).
11. A. Emadi, "Linear-variable optical filters for microspectrometer application," PhD Thesis, Technical University of Delft (2010).
12. V. Krajicek and M. Vrbova, "Laser-induced fluorescence spectra of plants," Remote Sens. Environ. **47**(1), 51–54 (1994).
13. K. Burns, K. B. Adams, and J. Longwell, "Interference measurements in the spectra of neon and natural mercury," J. Opt. Soc. Am. **40**(6), 339–344 (1950).
14. NIST atomic spectra database, Online: *http://www.nist.gov/pml/data/asd.cfm*

#155272 - $15.00 USD Received 28 Sep 2011; revised 14 Nov 2011; accepted 29 Nov 2011; published 21 Dec 2011

15. M. P. Wisniewski, R. Z. Morawski, and A. Barwicz, "Algorithms for interpretation of spectrometric data- A comparative study," Instrumentation and Measurement Technology Conference, 2000. IMTC 2000. Proceedings of the 17th IEEE, **2**, 703–706 (2000).
16. D. Massicotte, R. Z. Morawski, and A. Barwicz, "Kalman-filter-based algorithms of spectrometric data correction-Part I: an iterative algorithm of deconvolution," IEEE Trans. Instrum. Meas. **46**(3), 678–684 (1997).
17. M. H. Hayes and H. Monson, "Recursive least squares," in *Statistical Digital Signal Processing and Modeling* (Wiley, 1996), ch. 9.4.
18. S. Grabarnik, A. Emadi, H. Wu, G. de Graaf, and R. F. Wolffenbuttel, "High-resolution microspectrometer with an aberration-correcting planar grating," Appl. Opt. **47**(34), 6442–6447 (2008).

1. Introduction

On-chip optical microspectrometers have huge potential in applications that cannot be served with conventional bulky and expensive spectroscopic instruments [1]. For instance, optical analysis of the blood of a patient for concentrations of hemoglobin, glucose, toxin and other components without interaction with a central laboratory could be considered, which would allow a rapid diagnosis at the point-of-care or even at home [2].

Microspectrometers can be realized by integration of different optical filters on an array of photodetectors in a CMOS-compatible fashion when using a post-process [3]. The benefits of the filter approach, as compared to grating-based systems, are: Firstly, a strongly reduced dependence of the spectral resolution on the numerical aperture of the optical system, as is shown in this paper. This implies that a design would become possible in which a higher numerical aperture is achieved at a specified resolving power. Secondly, the deposition of the optical filters can be implemented as a post-process, which offers the opportunity of a fully IC-compatible process for fabrication of single-chip microspectrometers. The main limitation of this approach is that the benefits are significant only in case the spectrometer is designed for operation over a relatively narrow spectral band. This feature does limit the scope of applications, however makes the microspectrometer particularly suitable in applications that require the spectral analysis around an absorption line.

The spectral resolving power of a multiple spectral filter-based microspectrometer is limited by the number of different optical filters that can be realized. Increasing the resolving power requires an increased number of different optical filters. In previously reported research selective back-etching of the optical resonator layer in a Fabry-Perot (FP) type of optical filter in several steps was used for fabrication of different filters on top of an array of CMOS photodiodes [3, 4]. The minimum number of lithography steps required to result in N optical resonators of different thickness (which is required for N different spectral channels) is $^2\log N$. This approach becomes impractical for a large value of N, especially when considering the thickness tolerances in the deposited or back-etched layers. A solution is the application of a Linear-Variable Optical Filter (LVOF). Figure 1 shows the schematic of a LVOF.

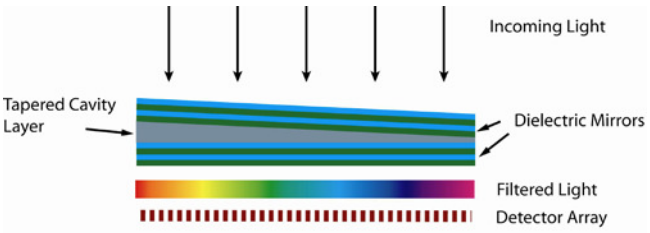

Fig. 1. A schematic view of a tapered Fabry-Perot type of Linear-variable Optical Filter.

A LVOF is in principle a FP type of filter in which the thickness of the resonance cavity changes linearly along its length, resulting in principle in an unlimited number of different FP filters [5]. Hence, the number of separate spectral channels depends solely on the number of the elements in the photodetector array. The useful number of bands depends on the finesse of the FP filter unless signal processing is applied, as implemented in this paper. Integration of a LVOF with a detector array can result in a robust, high-resolution on-chip microspectrometer. This paper covers different aspects for realization of such microspectrometers. Parts of this

#155272 - $15.00 USD Received 28 Sep 2011; revised 14 Nov 2011; accepted 29 Nov 2011; published 21 Dec 2011

work, such as the initial idea [6, 7] and the fabrication technique [8], have been published before. This paper covers all the design issues in detail, whereas the fabrication is summarized. The emphasis is on the spectral measurements and the discussion on free spectral range and resolution.

The operating spectral bandwidth of a LVOF-based microspectrometer is typically less than that of a grating-based microspectrometer. This limitation is due to the small bandwidth over which the dielectric multilayered structure of the FP mirrors can be designed to be highly reflective. The maximum free spectral range (FSR) is half the reflection bandwidth of the layers and is reduced by increasing the resonance order of the FP structure [9].

The thickness variation of the cavity layer of the LVOF is in the order of a quarter of the central wavelength of the LVOF. Since the length of the LVOF strip typically extends over several mm, a very small taper angle, ranging from 0.2° to 0.002°, needs to be realized in an IC-compatible process. This is the main technological challenge in the fabrication of an IC-compatible LVOF. A process based on reflow of a patterned layer of photoresist has been developed for the fabrication of such tapered layers and is presented in [10].

2. Design and fabrication of an LVOF-based microspectrometer for the visible spectrum

The design of a LVOF-based microspectrometer is complicated by the conflicting requirements of high resolving power and large free spectral range (FSR). The operating order, N, of a Fabry-Perot device can be expressed as: $N = 2nd/\lambda_o$ or $N = d/(2\times QWOT)$, where λ_o denotes the reference wavelength in free space, n is the refractive index of the cavity, d is the thickness of the cavity and QWOT (Quarter Wavelength Optical Thickness) is a quarter of the reference wavelength of the cavity. Higher resonance orders result in a smaller FWHM (Full Width Half Maximum), meaning sharper transmission peaks and thus a high resolving power. However, a high value for N also results in a reduced operating bandwidth of the LVOF: the Free Spectral Range (FSR).

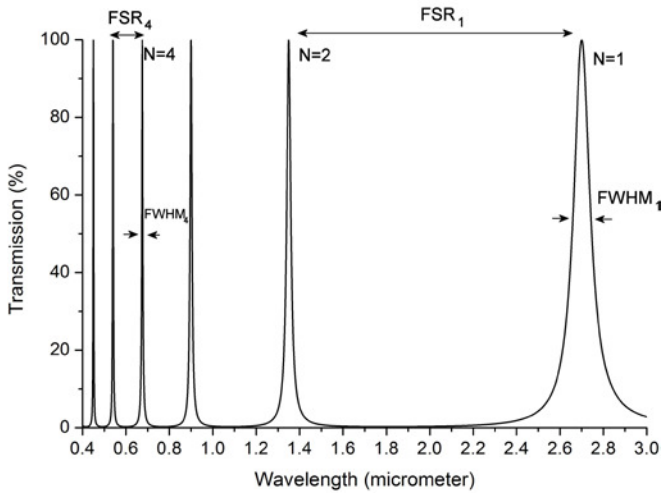

Fig. 2. Simulated transmission of a FP filter with R = 0.9, n = 1.5 and d = 900 nm. Both FSR and FWHM reduce with increasing resonance order, N.

The design is constrained by the ability to meet both the specifications on resolving power and FSR at a given value for N. This is illustrated in Fig. 2, which is the simulated transmission through a FP filter with d=900 nm, n=1.5 and mirror reflectivity R=0.9.

The FSR is the spectral bandwidth in which the FP filter of a certain order can be used without the presence of transmission peaks of different order. At any given order of resonance, N, the transmission peak of the order N+1 is always closer than the peak of the order N-1. Therefore, we can define the FSR for order N as the distance between the peaks of order N and N+1. This FSR_N can be expressed as [9]:

#155272 - $15.00 USD Received 28 Sep 2011; revised 14 Nov 2011; accepted 29 Nov 2011; published 21 Dec 2011

$$\mathrm{FSR}_N = \frac{2nd}{N(N+1)} \tag{1}$$

Also from the definition of finesse, f, results [11]:

$$f = \frac{FSR}{FWHM} = \frac{\pi}{2a\sin(1/\sqrt{F})} \rightarrow FWHM_N = \frac{4nda\sin(1/\sqrt{F})}{\pi N(N+1)} \tag{2}$$

Where F is the coefficient of finesse and depends on the reflectivity of the FP mirrors as: $F=4R/(1-R)^2$.

Dielectric multi-layers are used in a practical FP filter to build mirrors and the multi-layers are reflective over a certain spectral range. Hence, only the resonance transmission peaks within the reflective bandwidth of the multi-layers are observed. However, the above-mentioned equations remain valid.

When a LVOF operates over a spectral range that is smaller than FSR, at each position along its length (which is equivalent to a particular cavity width) there is only one resonance peak that can pass through. This situation prevails in the narrowband implementation of the LVOF-based microspectrometer that is presented in this paper. However, when the LVOF is intended to operate over a spectral range that is wider than the FSR, for some positions along its length (for some cavity thicknesses) there is more than one resonance transmission peak than can pass through. This effect is demonstrated in this paper in the wideband implementation of the LVOF-microspectrometer. As is shown in Fig. 1 and confirmed by Eq. (2), the two resonance peaks from two neighboring resonance orders have different FWHM. This effect is used for characterizing the wideband implementation of the LVOF-based microspectrometer based on an appropriate and well-defined optical input provided by a monochromator. However, an unambiguous response to an arbitrary spectrum is not possible. In sections 5 and 6 of this paper, both situations are discussed.

The multi-layered filter used for the LVOF is designed for operation in the 570 nm – 720 nm spectral range and the required thickness of the layers is shown in Table 1. This wavelength range contains the essential information in applications such as fluorescence spectroscopy of plants and H-α spectroscopy [12]. The performance characterization of the LVOF and the resulting microspectrometer in this wavelength range can be tested using a Neon lamp, which has most of its major emission lines in this wavelength range [13, 14].

The designed LVOF operates at the 4th order to meet the resolving power specification, which is incompatible with the coverage of the entire visible spectrum. Therefore, two special cases are pursued. The first one is a relatively wide band microspectrometer intended for 580 nm – 720 nm spectral range, whereas the second is for a smaller bandwidth of 615 nm – 680 nm. In both cases signal processing is used to achieve the highest possible spectral resolution, as is explained in Section 4.

The transmission spectra of the LVOF are plotted in Fig. 3 for three different values of the cavity width. The maximum reflecting bandwidth of a Bragg reflector, which is the basic element in the structure of the LVOF, can be calculated as:

$$\frac{\Delta\lambda}{\lambda_0} = \frac{4}{\pi} a\sin\left(\frac{n_2 - n_1}{n_2 + n_1}\right) \tag{3}$$

In which $\Delta\lambda$ is the maximum reflecting bandwidth, λ_0 is the reference wavelength and n_2 and n_1 are refractive indexes of the dielectric materials. Maximum value for Free Spectral Range (FSR) in turn is $\Delta\lambda/2$. TiO_2 and SiO_2 are selected as the high-n and low-n dielectric materials respectively. These two materials were the available dielectric materials with the highest refractive index difference. The refractive index of TiO_2 is about 2.25 and the refractive index of SiO_2 is about 1.45 in the visible spectral range. Applying this equation, results in $\Delta\lambda$ = 720 nm – 470 nm = 250 nm. This is the reflection bandwidth of the Fabry-Perot mirrors, which is inherent to the use of dielectric materials. The operating wavelength

#155272 - $15.00 USD Received 28 Sep 2011; revised 14 Nov 2011; accepted 29 Nov 2011; published 21 Dec 2011

range is in between 470 nm and 720 nm. The maximum possible FSR is $\Delta\lambda/2$ = 125 nm. However, the Fabry-Perot structure of the LVOF is intended for use at a higher-order mode.

Table 1. Layers thicknesses of multilayered UV Linear Variable Filter

Layer #	Material	Thickness (QWOT)	Thickness (nm)
Substrate	Glass	-	-
1	TiO_2	1	68.5
2	SiO_2	1	112
3	TiO_2	1	68.5
4	SiO_2	1	112
5	TiO_2	1	68.5
6	SiO_2	1	112
7	TiO_2	1	68.5
8	SiO_2	7.1-9.3	800-1050
9	TiO_2	1	68.5
10	SiO_2	1	112
11	TiO_2	1	68.5
12	SiO_2	1	112
13	TiO_2	1	68.5
14	SiO_2	1	112
15	TiO_2	1	68.5

Thus, the FSR is reduced to 100 nm, as is shown in Fig. 3. For each thickness of the cavity we can note that the filter has two or three transmission peaks in the $\Delta\lambda$ wavelength range. Consequently, one unique wavelength is transmitted at a particular position along the LVOF only if the operating spectral range of the LVOF is limited to the FSR. Since the entire spectral range should be considered in the measurements, two or three wavelengths are transmitted at each position along the LVOF (for each cavity thickness).

Two different types of LVOF have been fabricated and used for spectral measurements. The details are presented in the next section.

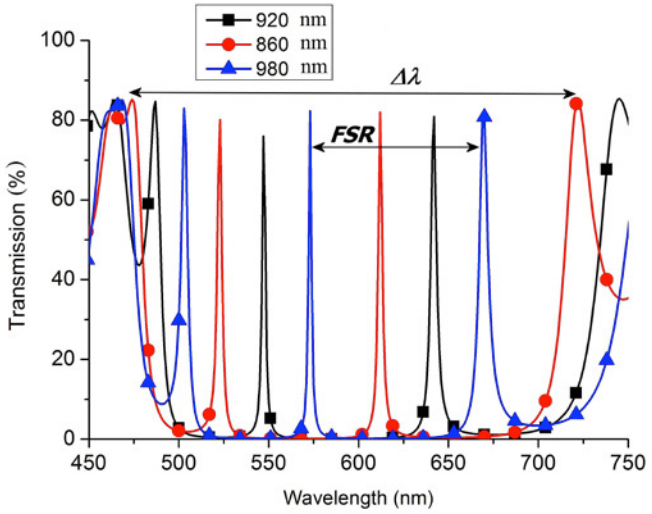

Fig. 3. Simulated spectra of LVOF for three values of the cavity thickness.

3. LVOF fabrication

LVOF fabrication is based on reflow of a specially patterned layer of resist. Figure 4 shows the process steps for the fabrication of an IC-Compatible LVOF. The process starts by deposition of the lower dielectric mirror stack and the oxide layer that results in the cavity

#155272 - $15.00 USD Received 28 Sep 2011; revised 14 Nov 2011; accepted 29 Nov 2011; published 21 Dec 2011

layer (layers 1-8 in Table 1). Photoresist is spin coated as the next step and lithography is applied to define the strip-like structure in the resist layer to be reflowed [8, 10].

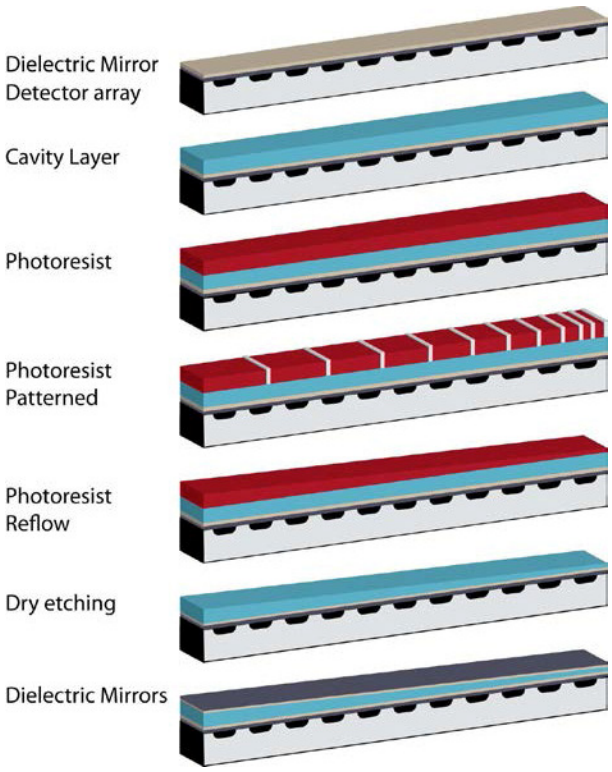

Fig. 4. Process flow for fabrication of Linear Variable Optical Filters.

A series of trenches of constant width and with variable spatial frequency or trenches of variable width and constant pitch are etched over the length of the strip of resist to vary the effective amount of resist per unit area. The subsequent reflow transfers this patterned resist layer into a smooth tapered resist layer. The topography of the tapered resist layer is transformed into the thick oxide cavity layer by an appropriate plasma etch. The process is completed by deposition of the top dielectric mirror stack (layers 9-15 in Table 1). This LVOF is fabricated on a glass substrate. However, fabrication directly on a CMOS detector chip as a compatible post-process is well possible.

4. Signal processing algorithm

There are several techniques for enhancing the spectral resolving power of spectrometers using signal processing [15–17]. In this paper an algorithm based on Least Mean Square (LMS) is used. The importance of data processing of the LVOF measurement results is discussed is discussed in this Section. The algorithm is based on an initial calibration step for spectral characterization. Calibration involves illumination of the LVOF with monochromatic light in an initial scan and recording the image that results from the transmission through the LVOF using a CMOS camera. The wavelength of the monochromatic light is swept over the entire spectral operating range of the LVOF. Figure 5 shows the set-up used for characterization of the LVOF. Imaging optics can be avoided in the simplest case and the LVOF filter can be put right on the top of the detector. The camera with the LVOF on top is placed in front of a monochromator and the wavelength of the light projected on the camera is swept with minimum possible step size in the entire operating wavelength range of the LVOF. The minimum wavelength step size in our case is 0.5 nm, which results from the specifications of the reference monochromator used (TRIAX 180).

#155272 - $15.00 USD Received 28 Sep 2011; revised 14 Nov 2011; accepted 29 Nov 2011; published 21 Dec 2011

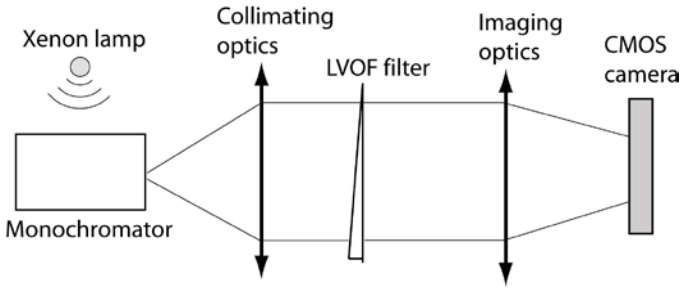

Fig. 5. Schematic for characterization of Linear Variable Optical Filters.

Basically, a LVOF operating within its FSR and specified by a certain FWHM (Full Width at Half Maximum Transmission) at each position yields a number of spectral channels equal to *N*= FSR/FWHM. For the LVOF with layers defined in Table 1 and transmission spectra shown in Fig. 3, this equals to 40 channels, each 2.5 nm wide. This is a significant advantage compared to Fabry-Perot filters with a discrete number of elements [3]. It is demonstrated in this section that it is possible to further enlarge the number of available spectral channels and thus the resolving power of the microspectrometer, using numerical analysis and signal processing.

The LVOF is placed on top of a detector array or camera with a 5.2 μm × 5.2 μm pixel size. From the characterization of the LVOF, it is observed that the illuminated region on the detector shifts over about 5 – 10 pixels (depending on the specifics of the camera and the LVOF) for each 1 nm of wavelength shift of the projected light. The basic idea is to use this fact for deriving a simple mathematical model, which allows us to detect small changes in intensity that is incident on the pixels.

Let us assume the spectral bandwidth of interest is divided into N spectral channels and we have N spectrally different (independent) detectors. The element C_{ij} in matrix C is defined as the response of channel *i* of the detector to component *j* in the spectrum (*i, j* = 1...N). The matrix C can be directly constructed from the data of a calibration measurement process. The maximum value of N is the number of the pixels on the camera, but can be limited by the spectral capability of the calibrating instrument (a monochromator). Hence, the measured intensity on the detector channels can be described as:

$$\begin{bmatrix} d_1 \\ d_2 \\ \dots \\ d_N \end{bmatrix} = \begin{bmatrix} c_{11} & c_{12} \dots c_{1N} \\ c_{21} & c_{22} \dots c_{21} \\ \dots & \dots \dots \\ c_{N1} & c_{N2} \dots c_{NN} \end{bmatrix} \begin{bmatrix} I_1 \\ I_2 \\ \dots \\ I_N \end{bmatrix} \quad \text{or} \quad D_{1N} = C_{NN} . I_{1N} \tag{4}$$

In which d_i denotes the measured intensity in channel *i* and I_i denotes the input light spectrum intensity in channel *i* that has to be calculated. In other words, Matrix D_{1N} is the raw data recorded on the camera pixels, matrix I_{1N} is the spectrum of incident light that has to be calculated and matrix C_{NN} is the calibration matrix which is determined during the calibration process. Let us consider once again calibration procedure shown schematically in Fig. 5. The light from a broadband source (Xenon lamp) is filtered by a monochromator and the selected wavelength is varied in the spectral range of interest for all the N spectral channels. For each spectral channel from the above equations, the calibration step is equivalent to deliberately having: $I = [0,0,...0,I_m = 1,0,...0]$ when channel *m* is selected from the monochromator. In this case the recorded intensities on the pixels give the values of column *m* of the C matrix:

#155272 - $15.00 USD Received 28 Sep 2011; revised 14 Nov 2011; accepted 29 Nov 2011; published 21 Dec 2011

$$\begin{bmatrix} d_1 \\ d_2 \\ \dots \\ \dots \\ \dots \\ d_N \end{bmatrix} = \begin{bmatrix} c_{11} & c_{12} & \dots c_{1N} \\ c_{21} & c_{22} & \dots c_{21} \\ \dots & \dots & \dots\dots \\ \dots & \dots & \dots\dots \\ \dots & \dots & \dots\dots \\ c_{N1} & c_{N2} & \dots c_{NN} \end{bmatrix} \begin{bmatrix} 0 \\ 0 \\ \dots \\ I_m = 1 \\ \dots \\ 0 \end{bmatrix} \rightarrow \begin{bmatrix} d_1 \\ d_2 \\ \dots \\ d_N \end{bmatrix} = \begin{bmatrix} c_{1m} \\ c_{2m} \\ \dots \\ c_{Nm} \end{bmatrix} \tag{5}$$

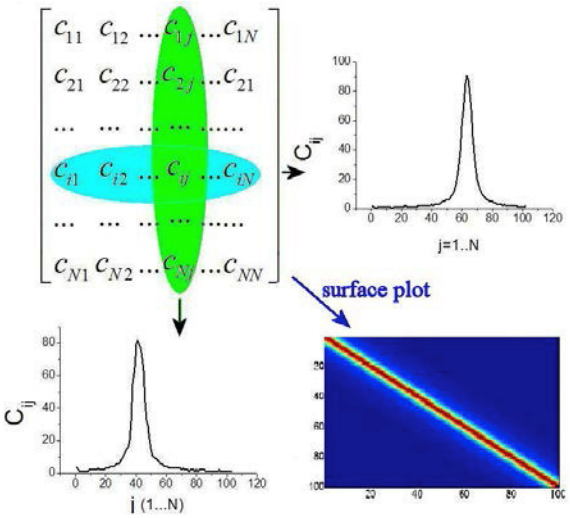

Fig. 6. Plotting rows and columns of the calibration matrix, the plot of the m-th column demonstrates the recorded intensity on the detector array for the m[th] monochromatic wavelength and the plot of n[th] row demonstrates the spectral response of the n[th] detector in the array. The surface plot of an ideal calibration matrix is strictly linear.

Repeating the procedure for all the N spectral channels results in determination of C_{NN} matrix. Plotting the rows and columns of the C matrix, Fig. 6, gives good understanding about the spectral response of the LVOF. The i^{th} row of the C matrix indicates the spectral response of the i^{th} channel in the detector array and the j^{th} column of the C matrix shows the recorded response of the detector array to the j^{th} monochromatic wavelength component.

The purpose of the calibration matrix can also be illustrated by making a surface plot of its rows and columns, as is also shown in Fig. 6. The surface plot of an ideal calibration matrix is strictly linear. This means a one to one relation between detector elements and spectral channels.

For a properly designed and fabricated LVOF, the matrix C has no singularity and it is in principle possible to take the inverse transform of the matrix (the matrix I can be calculated as: $I_{1N} = C_{NN}^{-1}.D_{1N}$). However, since matrix D is the result of actual measurement it contains uncertainties, which are primarily due to insufficient collimation and out of band signal. In case the uncertainties are significant as compared to the signal (low SNR), the direct calculation of matrix I would result in negative values in some of the spectral channels, which is nonphysical. In this paper an iterative procedure was implemented to calculate the best approximation of matrix I at the presence of uncertainties by minimizing matrix E:

#155272 - $15.00 USD Received 28 Sep 2011; revised 14 Nov 2011; accepted 29 Nov 2011; published 21 Dec 2011

$$E = \begin{bmatrix} d_1 \\ d_2 \\ \dots \\ d_N \end{bmatrix} - \begin{bmatrix} c_{11} & c_{12} \dots c_{1N} \\ c_{21} & c_{22} \dots c_{21} \\ \dots & \dots \dots \\ c_{N1} & c_{N2} \dots c_{NN} \end{bmatrix} \begin{bmatrix} \widehat{I}_1 \\ \widehat{I}_2 \\ \dots \\ \widehat{I}_N \end{bmatrix} \tag{6}$$

In which matrix $\hat{I}$ is an estimate of I. The Least Mean Square (LMS) algorithm is implemented based on the following equations:

$$\begin{aligned} E_n &= d - C\hat{I}_n \\ \hat{I}_{n+1} &= \hat{I}_n + \mu C E_n \end{aligned} \tag{7}$$

E_n denotes the error and $\widehat{I}_n$ denotes the estimate of the spectrum at each recursive step. μ is the convergence coefficient [17]. A higher value for μ results in faster convergence of the algorithm. However, it can also result in completely instability of the algorithm with diverging results. The goal of the algorithm is to decrease the mean square of E_n at each step. This results in the best possible estimate for the spectrum vector $\hat{I}$. The value of E_n does not go to zero due to noise and unwanted effects in the measurements.

For a narrowband application, in which the LVOF is operated within the FSR, the matrix C can be inverted. The algorithm described above converges into one unambiguous result. However, for a wideband application, matrix C is inherently not invertible. Although the algorithm converges, the result is not unambiguous and the algorithm may yield an incorrect wavelength peak.

Figure 7 shows one example. The LVOF is simultaneously illuminated with two monochromatic light sources, one tuned to the wavelength of resonance peak N and the other one to N-1. The figure shows the simulated intensity profile on the detector array after light passing through the LVOF. The solid line shows the illumination (intensity as recorded at the pixels) in case of a monochromatic component at *2nd/N*, whereas the dashed curve shows the illumination in case of a monochromatic component at *2nd/(N-1).* Similar to the FWHM we can define the width of such illuminated regions as HPLW (Half-Power Line Width). The HPLW is the width of the region where the intensity of light is half of its maximum. We can note the relation between HPLW and FWHM is expressed as: HPLW≈FWHM/θ, where θ is the angle of the slope of the LVOF. The width of the regions that are illuminated on the detector array by the different monochromatic light sources is different. This is due to the fact that they have different FWHM, as expressed by Eq. (2). This difference allows the algorithm to differentiate between these two peaks, even when a linear combination of these two monochromatic light spots is used for illuminating the detector.

#155272 - $15.00 USD Received 28 Sep 2011; revised 14 Nov 2011; accepted 29 Nov 2011; published 21 Dec 2011

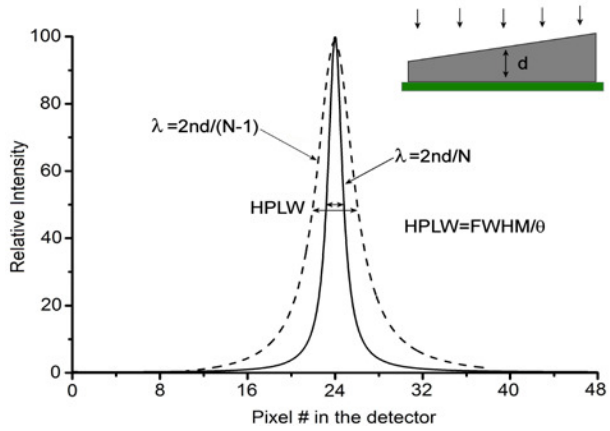

Fig. 7. Simulated intensity profiles on the detector for a wideband application, when two resonance peaks of different orders pass light at a particular location of the LVOF.

However, this is not the only possible solution. A non-chromatic broader light around the wavelength of the higher order would result in a very similar intensity profile on the detector. Therefore, the wideband application is not unambiguous. Nevertheless, this approach is suitable for spectral characterization of the wideband LVOF microspectrometer. The practical consequences are shown and discussed in more detail in section 6.

5. Spectral measurement for narrowband application

A LVOF based on Table 1 has been realized and used for spectral measurements. The cavity width varies along the length of this LVOF to yield resonators with thickness in the range between 850 nm and 980 nm. Therefore the transmission spectral peak is 600 nm at the thin end of the resonator layer and increases to 685 nm.

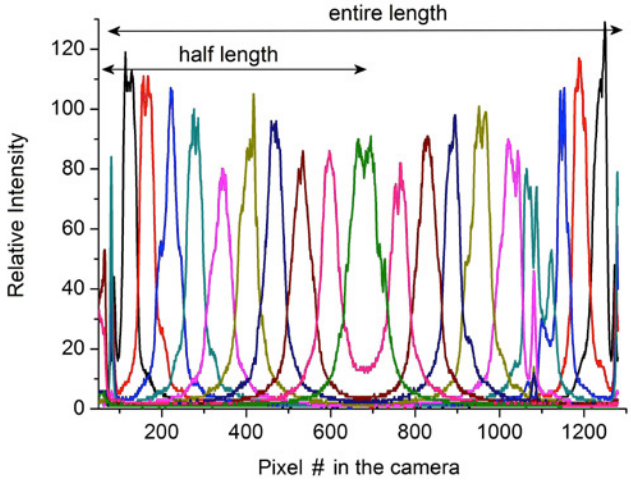

Fig. 8. Measured intensity profiles for monochromatic signals with 5nm separation, between 615 and 670nm (black = 615nm, red = 620nm, etc). Note that the entire length consists of two LVOF wedges with the thick parts meeting in the center, resulting in two peaks per wavelength. Also note that the numbers on the vertical axis are digitized pixels output.

This LVOF is mounted on top of a CMOS camera and the characterization (calibration) procedure discussed in the previous section is applied with 0.5 nm wavelength steps. Figure 8 shows the intensity profile on pixels for the spectral range in between 615 nm and 670 nm with 5 nm steps. The variation in the thickness of the deposited layers is typically 2% and mainly results in a shift of the designed resonance wavelength.

#155272 - $15.00 USD Received 28 Sep 2011; revised 14 Nov 2011; accepted 29 Nov 2011; published 21 Dec 2011

The peak transmission on the camera shifts by 12 pixels / nm. The Half Power Line Width (HPLW) is 40 pixels, which is equal to 240 µm in length. The structures are designed to have a hill-shape symmetric shape. The thickness increases linearly from the sides to the center, which is the thickest part of the LVOF. Therefore each structure includes two identical LVOFs at each side. The transmission peaks can be observed for both of the LVOFs from Fig. 8. At increasing wavelength the transmission peaks at each LVOF side of structure move closer to each other and towards the center of the filter structure.

The structure of an LVOF-based microspectrometer is shown in Fig. 9a, which is used as the starting point for the design of the required collimating optics. Light passes an aperture and collimating optics before being projected onto the LVOF, which is placed or deposited on the top of the detector. Equations (8) and (9) can be used to design the focal length of the collimating lens and the aperture size [8].

$$f = \frac{D}{2\mathrm{NA}}. \tag{8}$$

$$d = \frac{D\varphi}{\mathrm{NA}} \tag{9}$$

In which D is the size of the LVOF, f is the focal length of the lens and NA is the entrance numerical aperture, d is the diameter of the aperture and φ is maximum acceptable angle of incidence on the LVOF. Since these equations depend on φ, transmission through the multilayered Fabry–Perot filter (which can be at any position along the length of the LVOF) is simulated at different angles. Figure 9b shows the result.

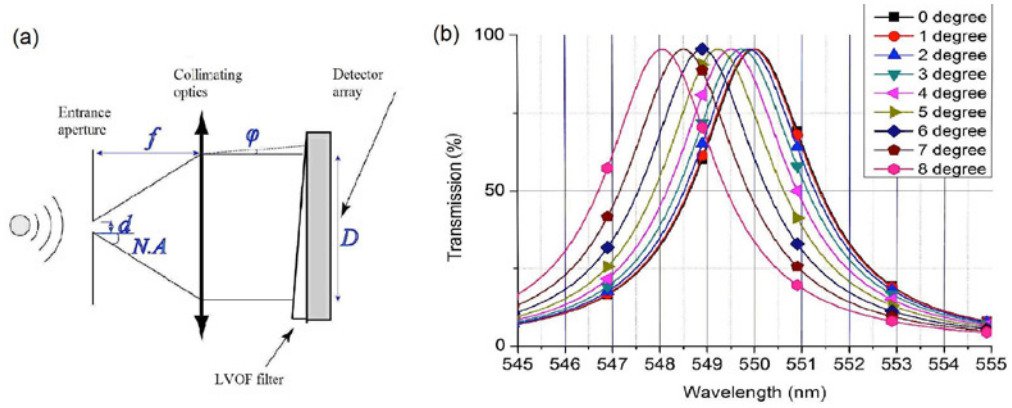

Fig. 9. a) Structure of a LVOF microspectrometer b) Simulated transmission through Fabry-Perot at different angles.

The figure shows that at an angle of incidence of 4° results in a shift in wavelength in the spectral response of 0.5 nm. At 6° this wavelength shift has increased to 1 nm. Based on these simulations φ can be selected. For example, for spectral accuracy better than 0.5 nm, φ = 3° is an acceptable choice. Hence, for our LVOF the following values are obtained: NA=0.4, f=12.5 mm, D=10 mm and d=1.3 mm. Consequently, the NA allows direct connection to a glass fiber (NA in the range 0.22 to 0.4, depending on type), which is not the as easily to achieve in grating-based systems. Based on these considerations, suitable collimating optics has been implemented in a C-mount holder to be put on the top of the CMOS camera, shown in Fig. 10.

#155272 - $15.00 USD Received 28 Sep 2011; revised 14 Nov 2011; accepted 29 Nov 2011; published 21 Dec 2011

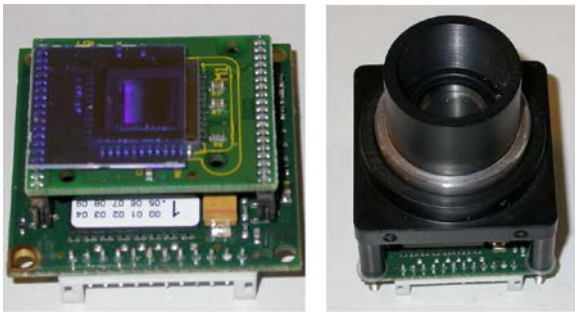

Fig. 10. LVOF mounted on the CMOS camera together with the C-mount holder for the collimating optics.

Although C-mount holder is relatively bulky, it is a convenient solution when parameters of collimating optics need to be changed for different experiments. In a final microspectrometer the C-mount holder has to be replaced by a miniaturized version.

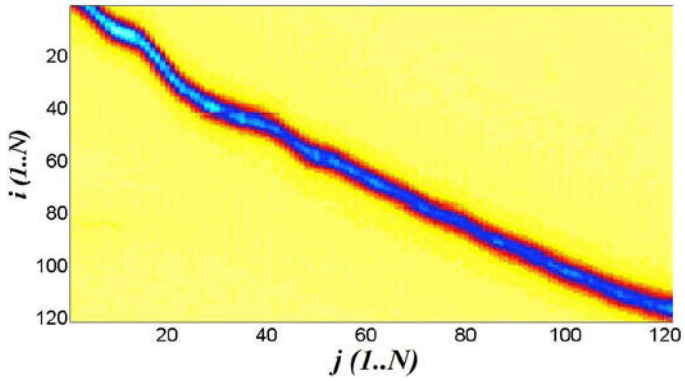

Fig. 11. Surface plot for calibration matrix.

Figure 11 shows a 2D plot of the values of the 121×121 calibration matrix obtained for this LVOF. The x-axis on the plot presents the different wavelength components (spectral input channels) and the y-axis presents the lines of pixels on the detector array (detector channels). The plot demonstrates the displacement of the illuminated region (at each wavelength) on the detector with linearly increasing wavelength. It is important to note the unique mapping of the spectral input channels onto the detector channels. This indicates that for each spectral band only one region of the detector channels is excited. This region is moving linearly along the length of the detector array as the wavelength is increased.

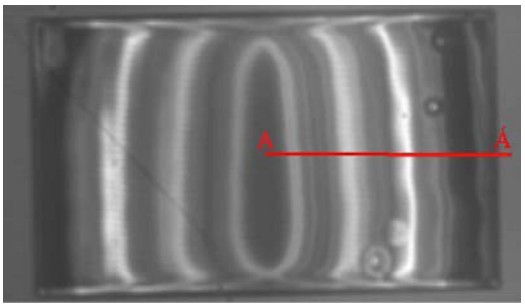

Fig. 12. Image recorded by the camera with narrowband LVOF illuminated by the Neon lamp.

Figure 12 shows the image recorded by the camera when the LVOF microspectrometer is illuminated by a Neon lamp. The out-of-band spectra of the Neon lamp, $\lambda < 610$ nm and $\lambda >$

#155272 - $15.00 USD Received 28 Sep 2011; revised 14 Nov 2011; accepted 29 Nov 2011; published 21 Dec 2011

670 nm, have been eliminated using three commercially available optical filters (Schott glass filters RG630, KG5 and an IR block filter). The pixel intensity profile from the recorded image is imported into the signal processing algorithm.

Figure 13 shows the recorded intensity profile of the pixels, as extracted from the recorded image in Fig. 12. Obviously this plot does not provide the required detailed spectral information about the spectrum of light, and the calibration and LMS algorithm discussed in the previous section have to be applied. Please note that the fabricated LVOF has two identical tapers on both sides resulting in two identical LVOFs with the thickest part in the middle of the combined structure. The data from only one side of this structure (one of the two LVOFs shown in Fig. 12 with line AÁ) is required for the LVOF microspectrometer concept as shown in Fig. 9a. Figure 13 shows the data when scanning over the up-going slope of the LVOF on the top of the detector. All spectral measurement results presented are based on a LVOF with only the up-going slope used.

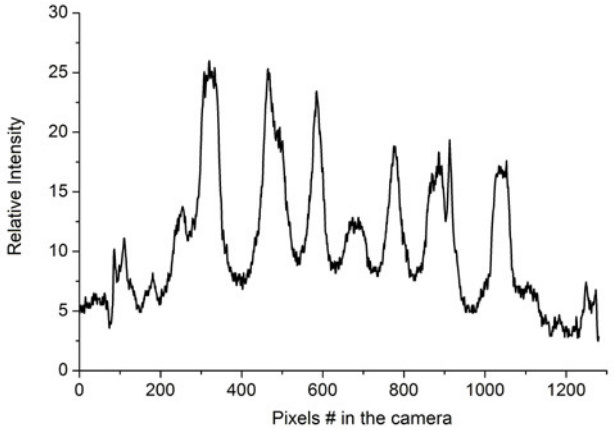

Fig. 13. Recorded intensity in the pixels along the AÁ line shown in the middle of the Fig. 12. The number of the pixels increases from the right side of the line to the middle of the image.

The spectrum is to be divided into N channels. Since we are limited by the spectral bandwidth of the light component provided by the monochromator used, the spectral width of each channel (the wavelength increment) is 0.5 nm. Covering 615 to 665 with 0.5 increments implies: $N = 101$. Consequently, N equally spaced pixels are selected along the length of the LVOF to result in the detector channels expressed by vector D_{IN} in Eq. (4).

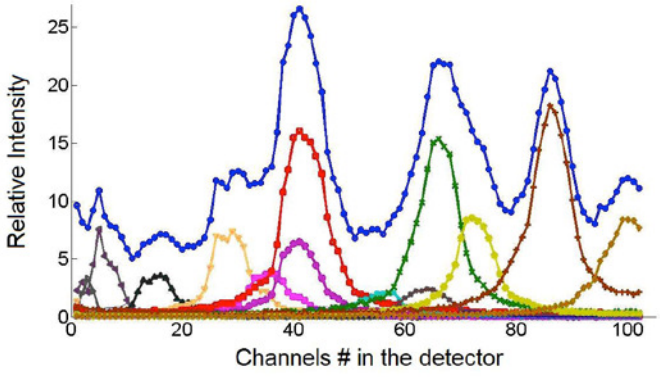

Fig. 14. LMS algorithm finds weighing coefficients in a way that the superposition of the curves converges to the recorded image. Note that channels are N equally spaced pixels in the detector array.

#155272 - $15.00 USD Received 28 Sep 2011; revised 14 Nov 2011; accepted 29 Nov 2011; published 21 Dec 2011

Extracting the spectrum from this data (in mathematical terms this is the calculation of I_{IN}), means finding weighing coefficients for measured intensity profiles in calibration in a way that the resulted superposition will converge to the recorded intensity in Fig. 13. This is illustrated in Fig. 14 by the top curve, with the dotted markers.

This curve is the result of the superposition of other smaller curves, which are the intensity profile curves measured in the calibration process, multiplied by their weighing coefficients found in the LMS algorithm. Mathematically, the line with the dotted markers is expressed by:

$$\begin{bmatrix} c_{11} & c_{12} & \dots c_{1N} \\ c_{21} & c_{22} & \dots c_{21} \\ \dots & \dots & \dots\dots \\ c_{N1} & c_{N2} & \dots c_{NN} \end{bmatrix} \begin{bmatrix} \widehat{I}_1 \\ \widehat{I}_2 \\ \dots \\ \widehat{I}_N \end{bmatrix}$$

The difference between the blue dotted curve in Fig. 14 and D_{IN} is the error in the measurement, which is expressed by vector E in Eq. (6). It is obvious that the level of noise and other unwanted effects in the measurement, determines the minimum achievable error. Figure 15a compares the blue dotted curve in Fig. 14 and D_{IN}. The numerical difference between these two is plotted in Fig. 15b.

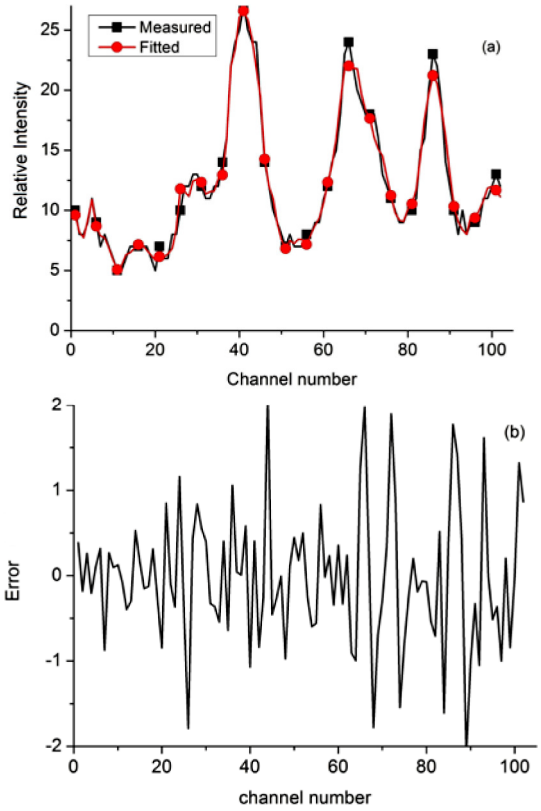

Fig. 15. a) Comparison between fitted and measured intensity in the channels b) Plot of the final error (difference between the fitted and measured pixels output).

Figure 16 shows a comparison between the calculated spectra of the Neon lamp from the LVOF data and the spectrum measured by a commercial spectrometer, used in [18], with 2

#155272 - $15.00 USD Received 28 Sep 2011; revised 14 Nov 2011; accepted 29 Nov 2011; published 21 Dec 2011

nm spectral resolution. There is good agreement between the two spectral measurements. The wavelength of each peak is written next to its marker in the figure in nm.

It can be seen that the LVOF has a higher resolving power as compared to a typical commercially available mini-spectrometer. The commercial spectrometer is unable to separate the different peaks at about 639 nm and the measurement shows a broad peak, whereas with the LVOF-based microspectrometer it was possible to resolve the smaller narrowly spaced peaks at 640.5 and 637 nm.

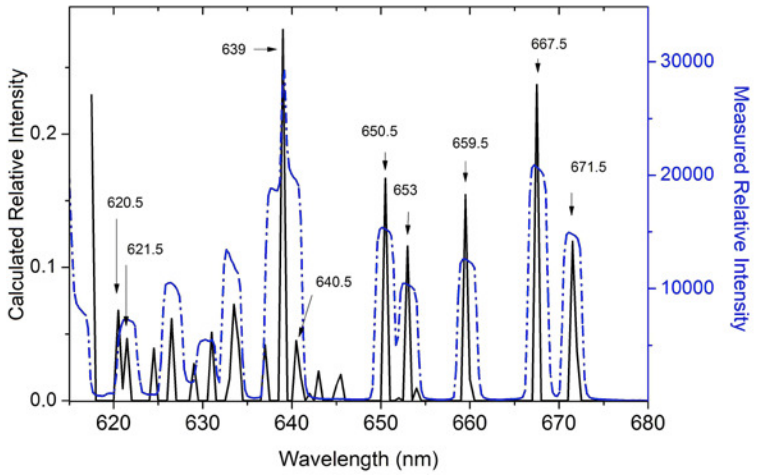

Fig. 16. Comparison of the spectrum of the Neon lamp that results from the LVOF (solid black line) with a commercially available spectrometer (blue dashed line), arbitrary units are used on the y-axis.

In order to make a better validation of the calculated spectrum, a comparison has been made with a grating-based microspectrometer reported in [18], which features a spectral resolving power of 0.7 nm. Figure 17 shows the comparison. Numbers given on the top of marker show the wavelength of the peak as calculated from the algorithm and the numbers in parenthesis show the wavelength from the references [13, 14].

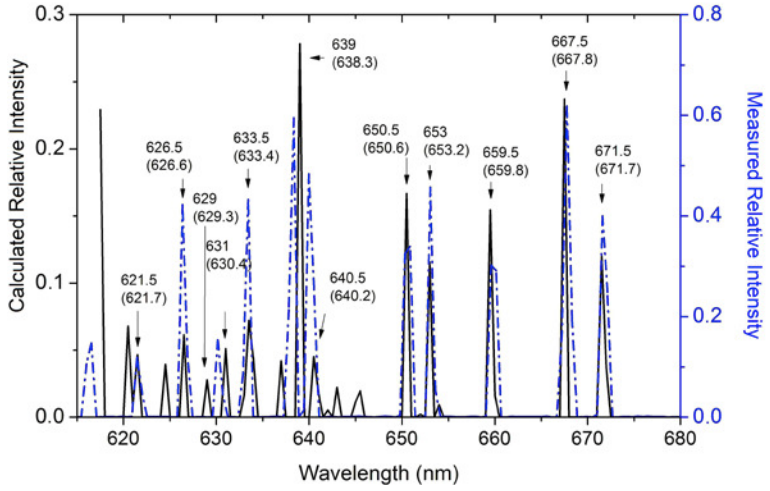

Fig. 17. Comparison between the spectrum of the Neon lamp calculated from LVOF (solid black line) and measured by a high-resolution grating-based microspectrometer (blue dashed line), arbitrary units are used on y-axis.

#155272 - $15.00 USD Received 28 Sep 2011; revised 14 Nov 2011; accepted 29 Nov 2011; published 21 Dec 2011

Note that there is good agreement between the peaks at 650.6 nm, 653.2 nm, 659.8 nm, 667.8 nm and 671.7 nm. The corresponding calculated wavelength as measured by the LVOF is less than 0.3 nm from the exact value. The difference is due to resolution of the calibration of the LVOF microspectrometer with spectral channels that are 0.5 nm apart.

The algorithm yields spectral peaks at 637.1 nm, 639 nm and 640.5 for the Neon spectral lines at 638.3 nm and 640.2 nm. These two spectral lines are calculated to be one strong spectral line (639 nm) together with two smaller lines (637.1 nm and 640.5). This is the largest error in the spectral measurements, which limits the absolute spectral accuracy to 0.7 nm. The main cause for this error is the out-of-band signal from the strong peaks of Neon below 615 nm, which are not completely filtered. The algorithm will try to find some peaks in a way that the overall recorded intensity on the detector array will match the calculations and hence an out-of-band signal inevitably results in additional peaks. In this case we can see that at 615 nm, which is the minimum wavelength of the band, the algorithm predicts a strong peak. This is a clear indication that shorter wavelength out-of-band signals are not properly filtered out.

Another limitation in these measurements is the small dynamic range of the CMOS camera, which outputs data in an 8-bit format. The quantization noise imported into the system from this error can also result in redundant peaks

6. Spectral measurement for wideband application

For the wideband design, LVOF layers with thickness as defined in Table 1 have been used. The cavity thickness varies from 800 nm to 1050 nm along the LVOF. The intention is to cover the entire spectral band of 570 nm to 720 nm. Therefore, at each position along the LVOF, the LVOF transmits two separate wavelengths in the spectral band of 570 nm to 720 nm.

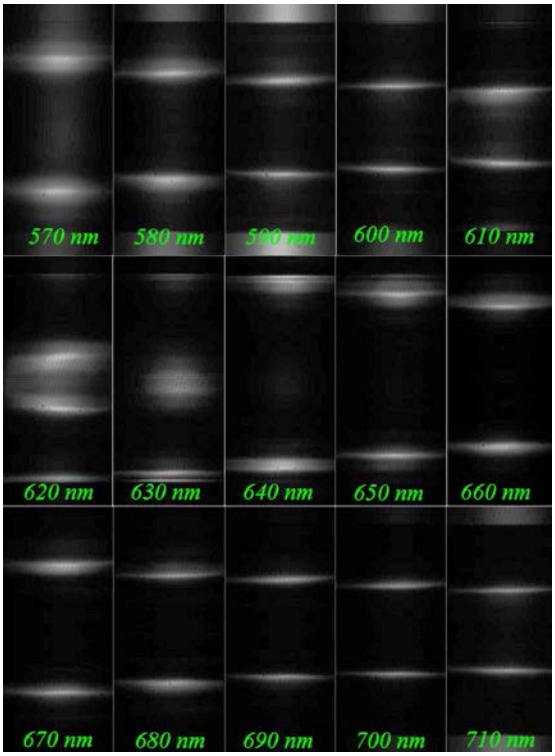

Fig. 18. Image recorded on the camera for LVOF to cover 570 nm – 740 nm for several monochromatic input signals.

#155272 - $15.00 USD Received 28 Sep 2011; revised 14 Nov 2011; accepted 29 Nov 2011; published 21 Dec 2011

The images recorded by the camera at different wavelengths are shown in Fig. 18. It can be seen that the illuminated part of the LVOF is at the two sides of the structure for 570 nm and moves at increasing wavelength towards the center, until at 630 nm spots reappear at the sides. It is important to note that this re-occurrence within the operating band makes it impossible to invert the C-matrix. Similar to previous section collimating optics is applied using a C-mount. An aperture of 1 mm is used together with an aspherical lens with focal length of 15 mm. An infra-red (IR) blocking filter has been placed on the aperture of collimating optics to remove the IR part of the Neon lamp from the spectrum. Moreover, a long-wavelength pass filter is used to block the spectrum below 570 nm. Figure 19a shows the image recorded by the camera when illuminated by the Neon lamp. Similar to the previous section, the intensity profile recorded by the pixels of the camera, Fig 19b, is the raw data and is fed to the signal processing algorithm.

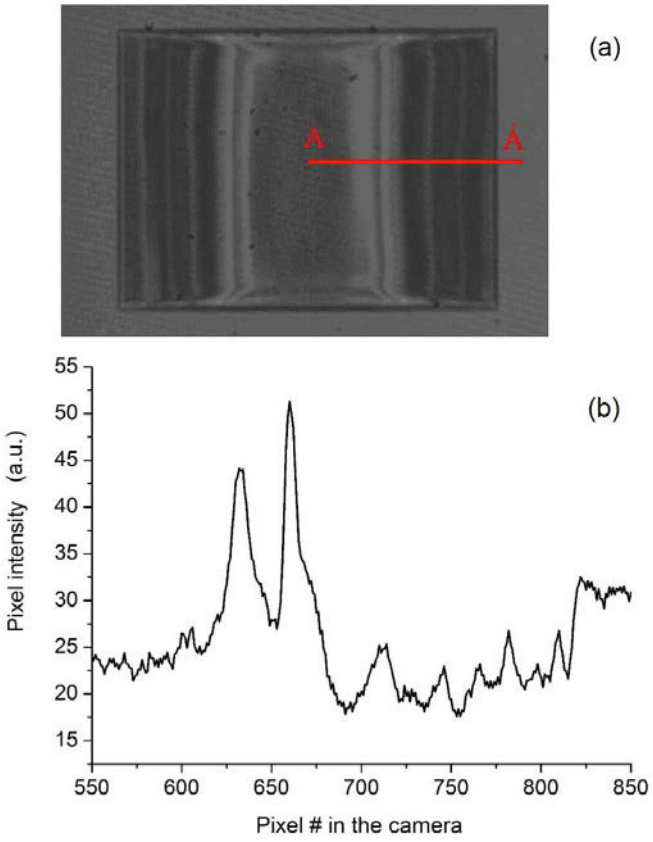

Fig. 19. (a) Recorded image on the LVOF camera and (b) recorded intensity in the pixels along the AÁ shown in the middle of the image. The number of the pixels increases from the right side of the line to the middle of the image.

The 2D plot in this case is a 171×171 calibration matrix C, which is plotted in Fig. 20. The plot demonstrates the movement of illuminated regions on the detector as the wavelength is linearly increased. Note that there is not a unique relationship between the spectral channels and the detector channels. This illustration of the calibration matrix shows that each detector channel responds to two different spectral wavelengths. However, these two peaks have different shape (FWHM) and because of that the algorithm is tested to check the possibility of separating these two peaks based on their shape.

Figure 21 shows the result of the LMS algorithm compared with the spectrum of Neon lamp measured by the commercial spectrometer used in [18]. There is good agreement

#155272 - $15.00 USD Received 28 Sep 2011; revised 14 Nov 2011; accepted 29 Nov 2011; published 21 Dec 2011

between the two spectra below 650 nm. The blind spectrum of the LVOF has been marked in the image and it can be seen that two of spectral line of the Neon lamp are neglected in that range. The neglected region is due to the fact that at each position along the detector two separate wavelengths can be calculated from the algorithm.

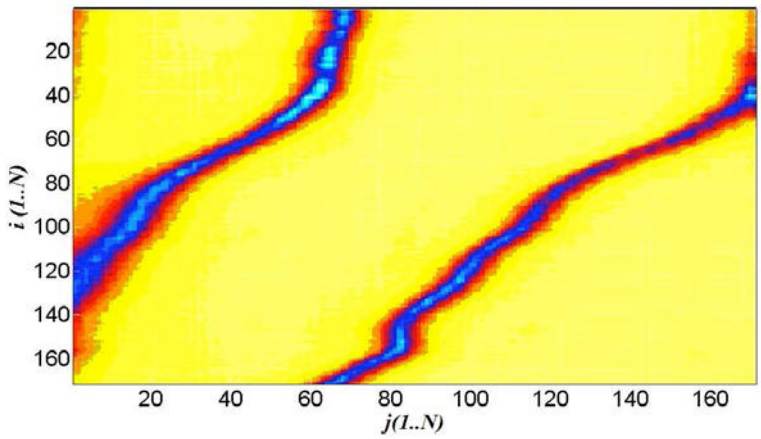

Fig. 20. Surface plot for calibration matrix.

Unwanted effects and error in the calibration causes the algorithm not to choose for the right wavelength in that region. The measurement indicates a spectral resolving power of 2.2 nm. In order to obtain more reliable result from the broadband application, we need to make sure that systematic errors such as out-of-band signal and small dynamic range are removed.

This result shows however that there is unavoidable uncertainty when using LVOF for wideband applications. This approach still can have application if we are interested in the intensities of several well-known peaks and when the spectrum of interest is partially known. However, for an arbitrary spectrum the result is ambiguous.

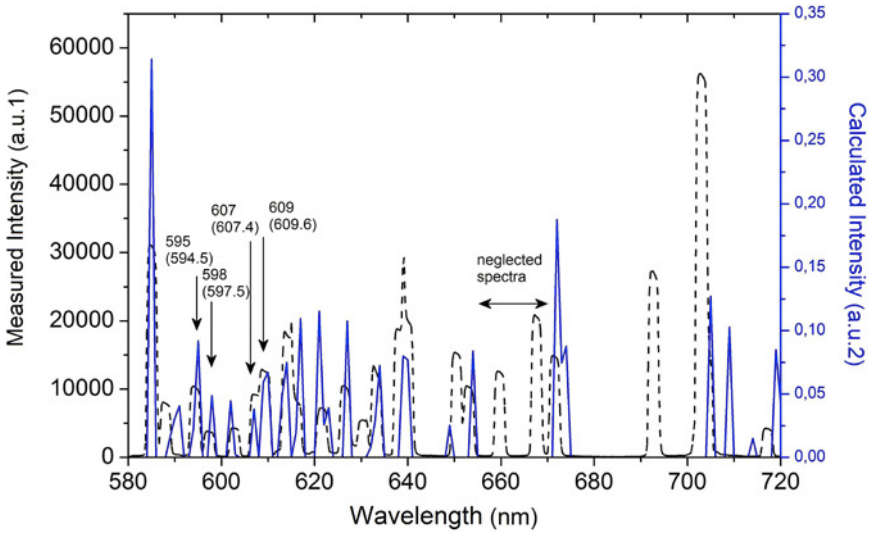

Fig. 21. Comparison between spectrum of the Neon lamp calculated from LVOF (blue solid line) and measured by a commercial spectrometer (black dashed line).

#155272 - $15.00 USD Received 28 Sep 2011; revised 14 Nov 2011; accepted 29 Nov 2011; published 21 Dec 2011

6. Conclusions

Two different types of LVOF-based microspectrometers have been realized for operation in the spectral range between 580 nm and 720 nm. The first LVOF realization was designed for narrowband operation to cover the spectral range from 615 nm to 680 nm, whereas the second one was designed to cover entire spectral range. The spectrum of a Neon lamp has been measured with both types of LVOF and the results are compared with the spectral measurements that were carried out using a commercially available spectrometer.

A simple LMS algorithm has been used to calculate the spectrum of the incident light on the LVOF microspectrometer from the image recorded on its camera. The results confirm that the best results can be achieved when using a LVOF in a narrowband application. A spectral resolution of 0.7 nm was achieved in case of a narrowband LVOF and for the wideband LVOF a spectral resolution of 2.2 nm was obtained. The signal processing algorithm relies on the calibration matrix, which is formed through a time-consuming calibration procedure. Therefore, critical to practical application are approaches that bring about the possibility of using one single calibration using only a subset of the spectral channels to construct this matrix.

The results also confirm that the main strength of LVOF microspectrometer is in applications in which the information is contained within a narrow band. This makes the LVOF-based microspectrometer particularly suitable for analyzing a narrowband spectrum around (several) transmission or absorption peaks. In wideband applications, the algorithm uses the fact that higher order peaks have a smaller FWHM. The algorithm, tries to find the best linear combination of the two to resemble the recorded data. This approach was used for characterizing the wideband device using a monochromator as illuminator. However, this approach can only be used when the spectrum of interest is partially known and yields ambiguous results in case of an arbitrary wideband input spectrum.

Improvements in the calibration technique are required for achieving higher spectral resolving power in case of large bandwidth application. The current procedure of signal processing for calculation and extraction of spectral information depends on full characterization and calibration of the LVOF applied. However, improving the procedure can highly simplify calibration. One alternative is to measure the spectrum of a calibrated source with a well-defined spectrum, and using a similar LMS algorithm to make a fitting to the parameters of the Calibration Matrix C. The initial values for C can be obtained from information about fabrication of the LVOF and based on optical simulations.

Acknowledgments:

This work has been supported by the Dutch technology Foundation STW under grant DET.6667. Some of the devices have been fabricated in Chalmers University of Technology through MC2ACCESS programme. The authors would like to thank Semen Grabarnik for valuable discussion and collaboration on this work.

#155272 - $15.00 USD Received 28 Sep 2011; revised 14 Nov 2011; accepted 29 Nov 2011; published 21 Dec 2011